Testosterone signaling through ZIP9 renders melanoma more aggressive in males than in females

Cristina Aguirre-Portolés[1], Riley Payne[2], Aspen Trautz[1], J. Kevin Foskett[2], Christopher A. Natale[1], Todd W. Ridky[1]*

[1]Department of Dermatology,
[2]Department of Physiology, Perelman School of Medicine, University of Pennsylvania, Philadelphia, PA. USA.
*Correspondence to: ridky@pennmedicine.upenn.edu

Summary

Androgen receptor inhibitors for prostate cancer also block the zinc transporter ZIP9, and thereby inhibit melanoma in males.

Abstract

Melanoma and most other cancers occur more frequently, and have worse prognosis, in males compared with females. Though sex steroids are thought to be involved, melanoma lacks classical androgen and estrogen receptors. Here we show that testosterone promotes melanoma proliferation by activating ZIP9 (*SLC39A9*), a zinc transporter that is not intentionally targeted by available therapeutics. This activity requires zinc influx, MAPK activation and YAP1 nuclear translocation. We demonstrate that inhibitors of the classical androgen receptor, also inhibit ZIP9, and thereby antagonize the pro-tumorigenic effects of testosterone in melanoma. In male mice, androgen receptor inhibitors suppressed growth of ZIP9-expressing melanomas, but had no effect on isogenic melanomas lacking ZIP9, nor on melanomas in females. These data suggest that ZIP9 might be effectively targeted in melanoma and other cancers by repurposing androgen receptor inhibitors that are currently approved only for prostate cancer.

Introduction

Cancer incidence and mortality are higher in males than in females in the U.S. and worldwide (*1*, *2*). In the U.S., males are 15% more likely to develop cancer, and 40% more likely to die from this disease than females (*2*, *3*). These sex differences were recognized as early as 1949 (*4*), are observed in the majority of cancer types from non-reproductive tissues, and remain even after controlling for known risk factors such as environmental and occupational exposures (*5*). While recent advances in modern targeted and immune therapeutics have markedly improved survival for both female and male melanoma patients (*6*), females still have more favorable outcomes (*2*, *5*). Incidence and rate death for melanoma are 1.6X and 2.5X higher, respectively, in males than in females in the U.S (*2*). Defining the mechanisms underlying the broad and persistent sex differences in cancer incidence and outcomes will address a major unresolved question in cancer pathobiology.

We previously showed that the female sex hormone estradiol inhibits melanoma proliferation and tumor growth *in vivo*. This effect is independent of biologic sex of the tumor, independent of classical estrogen receptors (ER), and results from activation of a nonclassical surface ER on melanocytes and melanoma cells called the G Protein Estrogen Receptor (GPER) (*7*, *8*). This work led us to consider whether male sex hormone signaling might also contribute to female vs. male differences in melanoma progression. Testosterone is the most abundant androgen and circulates at much higher levels in males (630 ng/dl) than in females (32 ng/dl) (*9*). Testosterone promotes proliferation *in vitro* in non-gonadal cell types including adipocytes (*10*), mouse skeletal muscle myoblasts (*11*), glioblastoma-derived cells (*12*), lung cancer cell lines (*13*) and melanoma (*14*). However, the receptor(s) mediating this activity and the corresponding downstream mechanisms are not defined. Also unknown is whether this androgen activity

observed *in vitro* is relevant to cancer progression *in vivo*. Here, we define a novel nonclassical testosterone signaling pathway in melanoma that preferentially promotes tumor growth in males, and demonstrate that this pathway can be effectively targeted with currently-available drugs.

Results

Melanoma tumors grow more quickly in male vs. female mice

To test whether preclinical melanoma models recapitulate the male vs. female survival disparity observed in humans, we first determined growth of human BRAF-driven melanoma WM46 cells, ($BRaf^{V600E}$; $CDK4^{R24C}$). Tumors consistently grew faster in immunodeficient SCID male mice compared with matched females (Fig. 1A). To test whether this phenotype extended to a genetically-engineered preclinical mouse model, we used murine YUMM1.7 cells ($BRaf^{V600E/wt}$;$Pten^{-/-}$$CdkN2a^{-/-}$) in syngeneic immunocompetent C57BL/6 mice. These tumors also consistently grew faster in male mice compared with matched females (Fig. S1A).

Testosterone, but not dihydrotestosterone, promotes proliferation in melanoma cells independent of the classical androgen receptor

Physiologic concentrations of testosterone promoted proliferation of both normal early passage primary human melanocytes and melanoma cells (Fig. 1B and Fig. S1B). In contrast, dihydrotestosterone (DHT) had no effect on proliferation of these cell types. The proliferative response to testosterone correlated with its concentration and was saturable, suggesting a specific receptor-mediated activity (Fig. 1C). None of the testosterone-sensitive primary melanocytes nor melanoma cells we tested express the classical androgen receptor (AR) (Fig. 1D), raising the possibility that a nonclassical hormone receptor is responsible for the testosterone activity.

Recently, the transmembrane zinc transporter *SLC39A9*/ZIP9 was discovered to bind testosterone in Atlantic Croaker (fish) cells (*15*). Importantly, testosterone was determined to have much higher affinity for ZIP9 than either DHT or androstenedione (*15*). The human ZIP9 homolog, encoded by the *SLC39A9* gene is broadly expressed in most cancers (Fig. S2A), normal human melanocytes, and all melanoma lines that we tested (Fig. 1D and Fig. S2B). ZIP9 transports zinc (Zn^{++}) across cell and organelle membranes into the cytoplasm and is the only steroid receptor known to directly regulate zinc homeostasis (*16*). Using the fluorescent Zn^{++}-specific probe FluoZin-3, we determined that testosterone induced a rapid increase in cytosolic free Zn^{++} concentration ($[Zn^{++}]_i$) in human melanoma cells (Fig. 1E), that was followed by a sustained elevation for at least 2 days in the continued presence of the androgen (Fig. 1F). We determined that Zn^{++} influx was necessary for testosterone-induced melanoma cell hyperproliferation, as treatment with the Zn^{++} chelator N,N,N′,N′-tetrakis (2-pyridinylmethyl)-1,2-ethanediamine (TPEN), blocked testosterone induced proliferation, while having no significant effect on its own (Fig. 1G and Fig. S3A). Although TPEN has high affinity for Zn^{++}, it has also has some ability to chelate copper (*17*). To test whether copper flux might contribute to testosterone effects on melanoma proliferation, we treated WM46 cells with $CuSO_4$, which had no significant effect on cell proliferation (Fig. S3B). Moreover, the highly specific copper chelator bathocuproinedisulfonic acid (BCS), did not affect the proliferative response to testosterone, nor did BCS affect testosterone induced Zn^{++} influx (Fig. 1H, Fig. S3C). After determining that Zn^{++} influx was necessary for testosterone-induced proliferation, we next asked whether increased Zn^{++} was sufficient to increase melanoma proliferation. Exogenous zinc pyrithione (also a Zn^{++} ionophore), and $ZnCl_2$ each increased melanoma proliferation (Fig. 1I). Other biologically-relevant divalent cations, Fe^{++} and Mn^{++}, known to be transported by other

ZIP family members (*18*), had no effect on proliferation (Fig. 1I). Together, these results demonstrate that testosterone, but not DHT, promotes melanoma proliferation that is dependent on Zn^{++} influx, and independent of the classic androgen receptor.

Testosterone signaling through ZIP9 promotes melanoma growth *in vivo*

To determine whether ZIP9 is the nonclassical androgen receptor that mediates testosterone effects in melanoma, we used CRISPR-Cas9 and gRNA targeting Slc39A9 exon1 to ablate ZIP9 in human WM46 melanoma and in murine YUMM1.7 melanoma cells. Isogenic clonal populations of parental ZIP9-expressing (wtZIP9) and ZIP9-null (ΔZIP9) cells were established. ZIP9 protein was completely absent in ΔZIP9 cells (Fig. 2A and Fig. S4A). ΔZIP9 cells did not respond to testosterone, whereas isogenic control clones responded similarly to parental cells (Fig. 2A and Fig. S4B). Consistent with this, exposure to testosterone or to exogenous zinc failed to increase $[Zn^{++}]_i$ in ΔZIP9 cells (Fig. 2B and 2C). Therefore, testosterone induces a rapid, ZIP9-dependent, increase in $[Zn^{++}]_i$ that is required for the hyperproliferation of melanoma-derived cells.

To test whether ZIP9 influences melanoma progression *in vivo*, WM46 wild-type and isogenic ΔZIP9 WM46 cells were subcutaneously injected into the flanks of SCID mice. Whereas wtZIP9 and ΔZIP9 tumors grew at similar rates in female mice, wtZIP9 tumors grew much faster than ΔZIP9 in the males (Fig. 2D). This observation suggests that ZIP9 is a major determinant of the male vs. female sex difference in melanoma.

Testosterone-induced melanoma proliferation through ZIP9 requires downstream MAPK and YAP1 activation

Although the studies detailed above show that testosterone promotes melanoma proliferation via ZIP9 dependent Zn^{++} influx, zinc is involved in myriad cellular processes, making it difficult to predict *a priori* which downstream signaling pathways are required for the testosterone activity

To start identifying these, we used a 447-element Reverse Phase Protein Array (RPPA) analysis of human WM46 melanoma cells treated with testosterone for 0, 30, 60 and 480 min. While the relative expression of most represented proteins was unaffected by testosterone, some were significantly under or overexpressed, including several with known tumor-promoting or tumor-suppressive functions (Fig. 3A, and Table S1). Downregulated proteins included 14-3-3ε, a tumor suppressor and negative YAP1 regulator previously implicated in liver, lung, and gastric cancers (*19*), and CDKN2A (p16), a cyclin-dependent kinase (CDK) inhibitor, and one of the most studied tumor suppressors (*20*). Upregulated proteins included key elements of tumor-promoting pathways, most notably phosphorylated ERK (T202; Y204) and YAP1. Importantly, ΔZIP9 cells displayed decreased basal levels of ERK phosphorylation compared with isogenic wild-type clones (Fig. S4C). MAPK activation was necessary for the hyperproliferative response to testosterone, as the specific ATP-competitive ERK1/2 inhibitor, Ulixertinib (*21*) (RVD-523) blocked the testosterone hyperproliferative response, while having no effect on the basal proliferation rate (Fig. 3B). Importantly, testosterone-dependent ZIP9 activation rendered WM46 cells more dependent on MAPK pathway activation, as their viability was compromised when they were treated with both testosterone and ulixertinib. In contrast, ΔZIP9 cells treated with both testosterone and ulixertinib proliferated at rates comparable to controls (Fig. 3B).

We determined that YAP1 activation is also required for the hyperproliferative response to testosterone. YAP1 is a transcriptional coactivator whose activity is largely regulated by its localization (*22*). Testosterone induced rapid YAP1 translocation from cytoplasm to nucleus in human melanoma cells (Fig. 3C and Fig. S4D). YAP1 subcellular localization is controlled largely by LATS, which phosphorylates YAP1 at Serine 127 and thereby retains YAP1 in the cytoplasm (*23*).

The YAP1 inhibitor dobutamine (Dob) also promotes phosphorylation of YAP at Ser127 (*24*). Consistent with this, testosterone-induced YAP1 nuclear localization and hyperproliferation were both blocked by Dob, which had no significant effect on its own (Fig. 3C, 3D). Testosterone promotion of YAP1 activity was evidenced by increased expression of a battery of YAP1 target genes including *CDC6*, *CYR61*, *LATS2* and *THBS1* (Fig. 3E). As expected, the testosterone-induced expression changes were blocked by Dob (Fig. 3E). Importantly, ΔZIP9 cells were refractory to both testosterone and Dob (Fig. S4E). We noted that YAP1 target-gene expression was lower in ΔZIP9 cells, suggesting that some degree of constitutive ZIP9 activity (in the absence of testosterone) helps maintain basal YAP signaling (Fig. S4F).

Pharmacologic ZIP9 blockade inhibits testosterone-driven melanoma growth *in vivo*

FDA-approved compounds can be repurposed to target ZIP9. Although specific ZIP9 inhibitors are not yet developed, molecular modeling and competition assays with fluorescent-tagged testosterone suggest that the androgen receptor inhibitor bicalutamide (BIC) competes with testosterone for ZIP9 binding to the same extracellular pocket and thereby acts as a competitive ZIP9 antagonist (*25*). Bicalutamide was developed and approved for prostate cancer and has now been largely replaced by enzalutamide (ENZ) and apalutamide (APA), which are structurally

related analogs with higher affinity for the androgen receptor and greater clinical efficacy against advanced prostate cancer (*26*, *27*). While ZIP9 was not known to be an androgen receptor at the time these drugs were developed, we show here that they are nonetheless effective inhibitors of testosterone effects in melanoma cells that lack the originally intended androgen receptor target, but that do express ZIP9. Each compound completely blocked testosterone-induced hyperproliferation and MAPK activation in several melanoma cell lines (Fig. 4A, 4B, 4C and Fig. S5A). Importantly, these agents alone (without testosterone) had no effect on cell proliferation (Fig. S5B). Consistent with a working model in which testosterone-induced Zn^{++} flux through ZIP9 is the critical mediator of the hyperproliferative response, bicalutamide significantly reduced Zn^{++} influx following testosterone exposure (Fig. S5C). Pharmacologic ZIP9 inhibition with apalutamide also blocked testosterone induction of YAP1 target genes including *CDC6*, *CRIM1* and *LATS2* (Fig. S5D).

Next, we tested whether apalutamide and related analogs inhibit melanoma *in vivo*. For this, we introduced wtZIP9 or isogenic ΔZIP9 human WM46 melanoma cells (which do not express AR) into SCID mice. Once-daily systemically administered apalutamide (20 mg/kg/day via oral gavage) significantly suppressed growth of wtZIP9 tumors in male mice and extended survival (Fig. 4D). Similar results were obtained when males were treated with bicalutamide (30mg/kg/day). Importantly, bicalutamide had no effect on wtZIP9 tumors in female mice (Fig. S5E). This strongly suggests that the anti-tumor activity results from inhibition of endogenous androgen signaling through ZIP9. Consistent with this mechanism, bicalutamide also had no effect on ΔZIP9 tumors in male mice (Fig. S5F). Together, these data show that nonclassical androgen signaling through ZIP9 promotes melanoma progression specifically in males.

Discussion

Although many have speculated that sex steroids contribute to sex differences in cancer pathobiology, definitive functional studies are lacking, and the mechanisms by which they contribute to the male-female cancer sex gap are largely unknown. We previously described the tumor suppressor activity of the nonclassical estrogen receptor GPER in melanoma (*7*). This finding led us to question whether circulating androgens in males might also contribute to the melanoma sex gap.

Testosterone promoted proliferation of melanoma cells in a saturable-dose-dependent manner. Surprisingly, the same cell lines did not respond to DHT, which is generally considered the more biologically active androgen. DHT displays 4-fold increased affinity than testosterone for AR, and it dissociates from AR three time slower than testosterone (*28*). Lack of response to DHT in melanoma is consistent with the absence of AR expression in the models used for this study, and perfectly consistent with our genetic data showing that ZIP9, which has much higher affinity for testosterone vs. DHT, is the mediator of testosterone effects.

Radio-labeled testosterone was used to definitively establish that ZIP9 binds to testosterone (*15*). Cell-based assays using fluorescent labeled testosterone demonstrate that bicalutamide competes with testosterone for ZIP9 binding, suggesting this interaction is pharmacologically accessible (*25*). Consistent with this, modeling studies suggest that bicalutamide binds to ZIP9 in the same pocket as testosterone and that this binding site is located on the extracellular surface of the protein. The functional significance of this testosterone-ZIP9 interaction in cancer, its contribution to the male vs. female sex gap, and the potential utility of targeting the interaction *in vivo* for cancer has not been explored previously.

There may be many drivers of the cancer sex gap in humans, including differences in immune surveillance (*29*). The relative influences of these various determinants are likely to vary with each tumor. Differences in immune surveillance do not appear to be a major driver of the differences in the melanoma models used for this study, as tumors progressed faster not only in male vs. female immunocompetent mice, but also in human melanomas grown in male vs. female SCID mice. We are therefore confident that the testosterone effects on melanoma in these models are dependent on ZIP9, but independent of B and T cell mediated anti-tumor activity. Consistent with this, ZIP9 expressing tumors respond to bicalutamide in SCID mice, and genetic ZIP9 depletion rescued the sex gap.

Bicalutamide is structurally similar to other members of the flutamide family including enzalutamide and apalutamide, which are better tolerated, and more effective against prostate cancer in people (*30*). Bicalutamide and apalutamide both inhibited melanoma growth in the experimental model used here.

As ZIP9 is widely expressed in nearly all tissues, it may be a major determinant of the sex disparity in outcomes not just for melanoma, but for many other cancer types as well (Supplementary Figure 6). The demonstration here that ZIP9 is pharmacologically accessible, suggests that ZIP9 may be a new eminently druggable therapeutic target (Fig. 4E), and that currently approved androgen receptor inhibitors might be useful alone, or in combination with current standard of care therapeutics for a wide range of cancers, especially those that disproportionately affect males.

Materials and Methods

CRISPR-Cas9 mediated ablation of Slc39A9

We used lentiviral transduction to deliver dox-inducible Cas9 and gRNA targeting exon 1 of Slc39A9 in human WM46 and murine YUMM1.7 melanoma cells. Transduced cells were selected with puromycin, and single cells subsequently isolated, expanded and examined for ZIP9 protein expression, compared to clones isolated in parallel in which control gRNA targeted GFP. The following gRNA sequences were used (5'-3'):

hZIP9_gRNA_Fw caccgTTGGTGGGATGTTACGTGGC:

hZIP9_gRNA_Rv aaacGCCACGTAACATCCCACCAAC.

Cell culture and proliferation assays

YUMM1.7 cells were purchased from ATCC (ATCC® CRL-3362™) and cultured in DMEM (Mediatech, Manassas, VA, USA) with 5% FBS (Invitrogen, Carlsbad, CA, USA) and 1% Penicillin-Streptomycin (Thermo Fisher Scientific. # 15140122). WM46 melanoma cells were a gift from Meenhard Herlyn (Wistar Institute, Philadelphia, PA, USA) and were cultured in TU2% media. Tumor cells were regularly tested using MycoAlert Mycoplasma Detection Kit from Lonza (Allendale, NJ, USA). For monitoring cell proliferation $10x10^5$ YUMM1.7 or $15x10^5$ WM46 cells were seed per well in 12-well Cell culture Plates. Cells were treated every second day and manually counted in triplicate using a hemocytometer. All the experiments were performed in cell populations that were in culture during a maximum of 3 weeks (5 passages in average) since thaw from the corresponding stock.

Zinc influx analysis

WM46 cells were loaded with 5 µM FluoZin™-3, AM, cell permeant™ (Thermo Fisher Scientific, #F24195), for 20 minutes then incubated in 2 Ca Tyrode's solution (in mM: 140 NaCl, 5 KCl, 1 $MgCl_2$, 2 $CaCl_2$, 10 glucose and 5 (Na) Pyruvate – pH 7.4) for 5-10 minutes at room temperature prior to imaging. Cells were imaged on a Nikon Ti microscope using a 20x/0.75 NA objective for fluorescence at 340 nm and 380nm excitation/515 nm emission (Ca^{2+}-free Fura2 or FluoZin™-3) and 380 nm excitation/515 nm emission (Ca^{2+}-free Fura2 FluoZin™-3). Coverslips were perfused at 1-3 mL/min following this protocol: Ca^{2+} Tyrode's (0-30 secs); Ca^{2+} Tyrode's + DMSO & 5 uM Zinc (30-90 secs); Ca^{2+} Tyrode's + Testosterone & 5□M Zinc (90-360 secs); Ca^{2+} Tyrode's + Testosterone + BIC & 5 uM Zn (360-470 secs); Ca^{2+} Tyrode's washout (470-500 secs). 100 milliseconds exposure images for each wavelength were collected every 2 seconds. For analyzing the long-term consequences of testosterone treatment, cells were treated with the androgen for 96 hours and then loaded FluoZin™-3. Cells were incubated with FluoZin™-3 following manufacturer recommendation and exposed to 400nM Zn pyrithione or $ZnCl_2$. Images were acquired with EVOS BLA. Fluorescence was quantitated using ImageJ (National Institutes of Health, Bethesda, MD, USA), and statistical analyses were performed using Graphpad Prism software.

Western blot, immunofluorescence and antibodies

Adherent cells were washed once with PBS and lysed with 8M urea containing 50mM NaCl and 50mM Tris-HCl, pH 8.3, 10mM dithiothreitol, 50mM iodoacetamide. Lysates were quantified (Bradford assay), normalized, reduced, and resolved by SDS gel electrophoresis on 4–15% Tris/Glycine gels (Bio-Rad, Hercules, CA, USA). Resolved protein was transferred to PVDF

membranes (Millipore, Billerica, MA, USA) using a Semi-Dry Transfer Cell (Bio-Rad), blocked in 5% BSA in TBS-T and probed with primary antibodies recognizing β-actin (Cell Signaling Technology, #3700. 1:4000, Danvers, MA, USA), ZIP9 (Cell Signaling Technology, #137205, 1:500), P-ERK (Cell Signaling Technology, Phospho-p44/42 MAPK (Erk1/2) (Thr202/Tyr204) (D13.14.4E) XP® Rabbit mAb #4370. 1:1000), ERK (Cell Signaling Technology, p44/42 MAPK (Erk1/2) (137F5) Rabbit mAb #4695, 1:1000), P-RB (Cell Signaling Technology, Phospho-Rb (Ser807/811) (D20B12) XP® Rabbit mAb #8516, 1:1000), and RB (Cell Signaling Technology, Rb (D20) Rabbit mAb #9313. 1:1000). After incubation with the appropriate secondary antibody (Rabbit Anti-Mouse IgG H&L (Biotin) preabsorbed (ab7074); Anti-mouse IgG, HRP-linked Antibody #7076. 1:2000) proteins were detected using ClarityTM Western ECL Substrate (Bio-Rad. #170-5060). All western blots were repeated at least 3 times. To monitor YAP1 nuclear translocation by Western blot analysis, nuclear fractionation was performed using protein lysis buffer containing 10mM HEPES, 1mM KCl, 1.5mM MgCl2 and 10%glycerol (Buffer A). After washing the adherent cells with DPBS, samples were resuspended in Buffer A and incubated for 5 minutes on ice in the presence of 0.1% Triton-X-100. After centrifugation, the nuclear fraction remained as a pellet while the supernatant corresponded to the cytosolic fraction. Nuclear fraction was washed with Buffer A. After centrifugation, the nuclear fraction was resuspended in RIPA buffer and samples were boiled for 5 min prior to sample loading. The cytosolic fraction was centrifuged for 15 min at 13500 rpm. Only the supernatant was kept after centrifugation. Western blot was performed as described before and the following antibodies were used for protein detection: β-tubulin (Cell Signaling Technology, β-Tubulin (9F3) Rabbit mAb #2128. 1:1000), PARP (Cell Signaling Technology, Rabbit mAb #9542. 1:1000), YAP1 (Cell Signaling Technology, YAP (D8H1X) XP® Rabbit mAb #14074.

1:1000). For immunofluorescence in adherent cells, samples were fixed with 4% paraformaldehyde (Affymetrix; #19943) for 7 min and permeabilized with iced-cold methanol. After blocking with 10% FBS:0.03%Triton-X100, primary antibodies were incubated overnight in blocking solution (β-actin and YAP1 antibodies detailed above). After three washes in DPBS:0.03% Triton X-100) cells were incubated with secondary antibodies for 45 min at room temperature (Goat anti-Mouse IgG (H+L) Highly Cross-Adsorbed Secondary Antibody, Alexa Fluor 594. Goat anti-Rabbit IgG (H+L) Highly Cross-Adsorbed Secondary Antibody, Alexa Fluor 488). Cells were rinsed with PBS-0.03% Triton three times and coverslips were mounted with ProLong Gold antifade reagent with DAPI (#P36935; Thermo Fisher Scientific). Images were captured using a Leica DM IL microscope and registered using LAS software. For fluorescence intensity quantification ImageJ software (National Institutes of Health, Bethesda, MD, USA) was used, and statistical analyses were performed with GraphPad Prism software.

Mice, subcutaneous tumors and pharmacologic treatments

All mice were purchased from Taconic Biosciences, Inc. (Rensselaer, NY, USA). Six- to eight-week old male and female C57BL/6NTac or IcrTac:ICR-Prkdcscid mice were allowed to reach sexually mature ages or to acclimatize for one week prior to being used in experiments. These studies were performed without inclusion/exclusion criteria or blinding but included randomization. Based on a two-fold anticipated effect, we performed experiments with at least 5 biological replicates. All procedures were performed in accordance with International Animal Care and Use Committee (IACUC)-approved protocols at the University of Pennsylvania. Subcutaneous tumors were initiated by injecting tumor cells in 50% Matrigel (Corning, Bedford, MA, USA) into the subcutaneous space on the right flanks of mice. 10 x 10^6 human WM46 cells

were used for each tumor. Oral administration of vehicle, bicalutamide (30mg/kg/day) or apalutamide (20mg/kg/day) was performed daily. 100µl of drug were administrated by oral gavage [10%DMSO:90%Vehicle (15% ethanol:85% sesame oil)]. Weight and health status of the mice as well as tumor growth were monitored daily. As subcutaneous tumors grew in mice, perpendicular tumor diameters were measured using calipers. Volume was calculated using the formula $L \times W^2 \times 0.52$, where L is the longest dimension and W is the perpendicular dimension. Animals were euthanized when tumors exceeded a protocol-specified size of 15 mm in the longest dimension. Secondary endpoints include severe ulceration, death, and any other condition that falls within the IACUC guidelines for Rodent Tumor and Cancer Models at the University of Pennsylvania.

Quantitative RT-PCR

RNA was extracted using RNeasy kit (Qiagen. #74104) following the manufacturer's instructions. cDNA was obtained using High Capacity cDNA Reverse Transcription Kit (Applied Biosystems #4368814). For quantitative real-time PCR, PowerUP™ SYBR™ Green Master Mix (Applied Biosystems #A25741) was used. ViiA 7 Real-Time PCR System was used to perform the reaction (Applied Biosystems). Values were corrected by actin expression. The $2^{-\Delta\Delta Ct}$ method was applied to calculate the relative gene expression. Primers used for the amplification are included in Table S2.

Statistical analysis

To optimize scientific rigor, each experiment included at least n=5 replicates, which provides 100% power to detect at least a 50% difference between groups with 95% confidence. For

experiments comparing two groups (treated vs control), significance was calculated using the Mann-Whitney test. For experiments with more than two groups, one-way ANOVA with Tukey's honest significance difference test was performed. Statistical analyses were performed using Graphpad Prism Software. Error bars represent standard error of the mean (SEM). **** p value<0.0001; *** p value<0.001; ** p value<0.005; * p value<0.01.

Acknowledgements

The authors thank the University of Pennsylvania Skin Biology and Disease Research-based center for analysis of tissue sections. **Funding:** T.W.R. is supported by grant from the NIH/NCI (R01 CA163566, R41CA228695), and by the Stiefel award from the Dermatology Foundation. This work was also supported in part by the Penn Skin Biology and Diseases Resource-based Center (P30-AR069589), the Melanoma Research Foundation, and R37 GM56328 to J.K.F**.** **Author Contributions:** C.A.P., R.P., A.T. performed the experiments. C.A.P., R.P. and J.K.F designed and performed the experiments to study zinc influx. J.K.F provided experimental material and reviewed the manuscript. C.A.P, C.A.N. and T.W.R designed experiments and wrote the article. **Competing interests:** C.A.P., C.A.N., and T.W.R., and are inventors on a provisional patent held by the University of Pennsylvania related to this work.

Figure legends and Figures

Fig. 1: Biologic sex and testosterone influence melanoma proliferation A. Tumor growth in SCID male and female mice bearing human melanoma derived tumors (WM46). Five mice per condition. Error bars represent standard error of the mean (SEM). **B.** Relative cell proliferation determined after 6 days of treatment with vehicle (DMSO), 100 nM testosterone (T) or 100 nM dihydrotestosterone (DHT). Human melanocytes (H.Mel.), WM46 human melanoma cells are shown. The graphs represent the average of three independent experiments. Error bars represent standard error of the mean (SEM). **C.** Relative cell proliferation of WM46 cells exposed to increasing concentrations of testosterone (T). **D.** AR and ZIP9 protein expression by Western blot. Human primary melanocytes, WM46, YUMM1.7 and human uveal melanoma (Mel.290) cells are shown. MCF7 breast cells was used as positive control for AR expression. **E.** Time-lapse analysis of Zn^{++} influx upon testosterone addition. FluoZin-3 was used as Zn^{++} reporter. **F.** Intracellular levels of Zinc after long-term testosterone treatment. **G.** WM46 relative proliferation in the presence of Zinc chelator (TPEN). **H.** WM46 relative proliferation in the presence of copper chelator (BCS). **I.** WM46 relative proliferation in the presence Zinc salts, FeSO4 and MnCl2. **** p value<0.0001; *** p value<0.001; ** p value<0.005; * p value<0.01.

Fig 2: ZIP9 mediates testosterone effects in melanoma. A. Relative cell proliferation in clonal populations of WM46 wtZIP9 and ΔZIP9 exposed to increasing concentrations of testosterone (T) in vitro. The graph represents the average of three independent experiments. Error bars represent standard error of the mean (SEM). **B.** Intracellular levels of Zinc in human melanoma ΔZIP9 cells. Graphs represent the average of three independent experiments. Error bars represent standard error of the mean (SEM). **C.** Relative cell proliferation in the presence of testosterone (T), Zinc chelator (TPEN) and ZnCl2. The graph represents the average of three independent

experiments. Error bars represent standard error of the mean (SEM). **D.** WM46 derived subcutaneous tumor growth in SCID male and female mice (wtZIP9 and ΔZIP9).

**** p value<0.0001; ** p value<0.005; * p value<0.01.

Fig. 3: Testosterone induced melanoma hyperproliferation requires ZIP9 and activation of MAPK and YAP1. A. RPPA analysis displaying changes in protein expression in WM46 human melanoma cells following exposure to testosterone (T). Down-regulated proteins are shown in green; Up-regulated proteins in light red. Control proteins showing no fold-change when compared to vehicle-treated cells are shown in blue. **B.** Relative cell proliferation under pharmacologic ERK1/2 inhibition with 50nM RVD-523 (ERKi) alone or in combination with testosterone. wtZIP9 and ΔZIP9 WM46 cells are shown. Western blot shows levels of phosphorylation of the ERK target RSK in wtZIP9 and ΔZIP9 WM46 cells (Ei corresponds to ERKi). **C.** YAP1 immunodetection after 30 minutes of exposure to testosterone (T) and/or dobutamine (Dob). YAP1 is shown in green; β-actin is shown in red; DAPI marks DNA in blue. Scale bar=25mm. **D.** Relative cell proliferation of wtZIP9 and ΔZIP9 WM46 cells after treatment with testosterone (T) and/or dobutamine (Dob). **E.** Relative mRNA expression of YAP1 and a battery of YAP1 target genes after 24 hours in the presence of testosterone and/or dobutamine. **** p value<0.0001; *** p value<0.001, ** p value<0.005; * p value<0.01.

Fig. 4: Pharmacologic ZIP9 blockade inhibits melanoma *in vivo*. A. Relative cell proliferation in human-derived melanoma cells (WM46) in the presences of testosterone (T) and/or AR inhibitors (BIC:Bicalutamide; ENZ:Enzalutamide; APA:Apalutamide). Western blot showing protein levels in WM46 cells treated with testosterone, BIC and Zinc chelator (TPEN). **B.** Relative cell proliferation in human and murine derived melanoma cells treated with T in combination with Apalutamide. **C.** Relative cell proliferation of WM46 wtZIP9 cells and ΔZIP9

cells in the presence of T and APA. **D.** Tumor growth in SCID male mice bearing WM46 derived subcutaneous tumors (APA treatment: 20mg/kg/day via oral gavage). **E.** ZIP9 activation promotes ERK phosphorylation and induces YAP1 nuclear translocation. AR inhibitors [represented in the figure by apalutamide (APA)] block testosterone effects through ZIP9 inactivation.

Figure 1

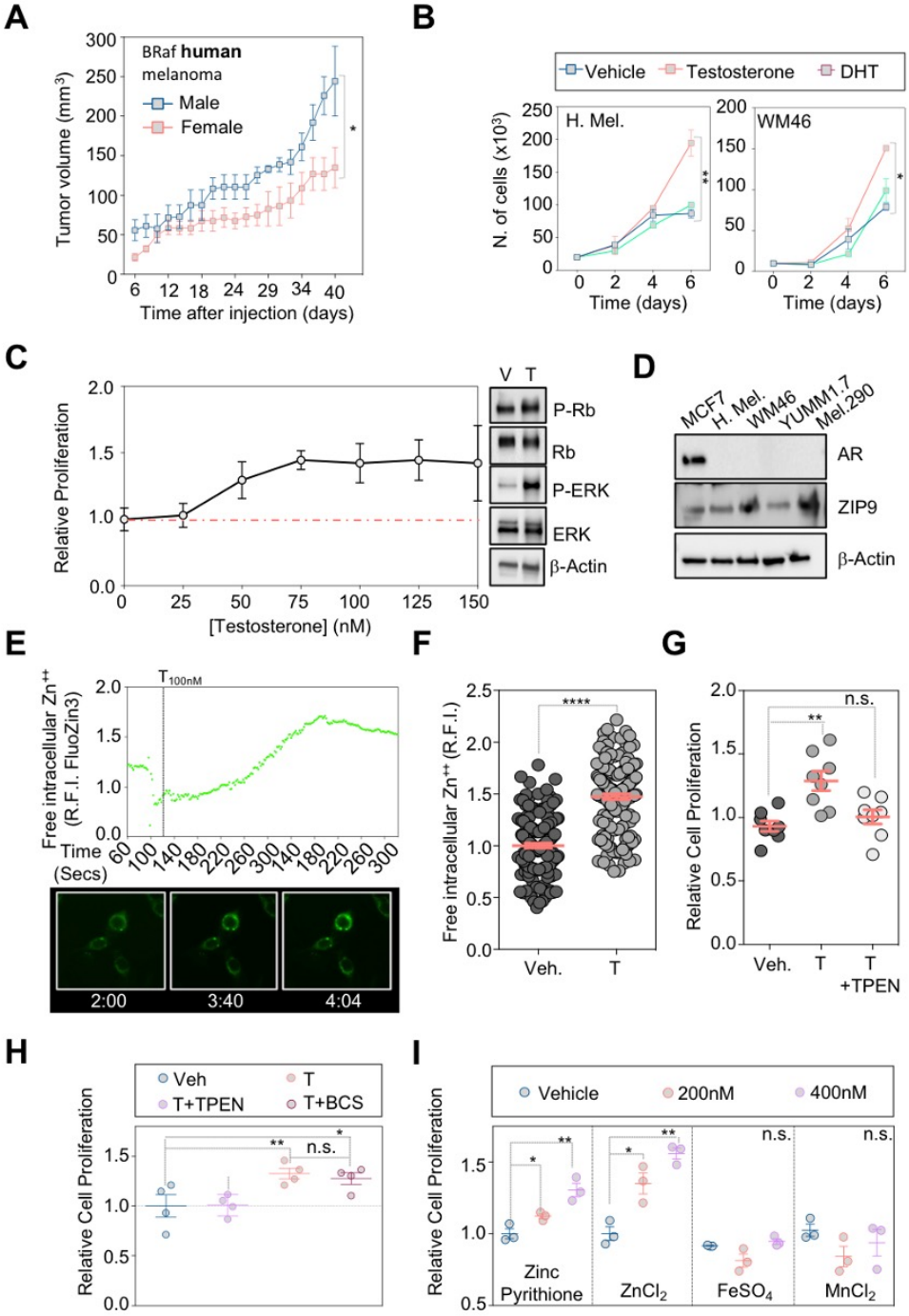
A
BRaf human melanoma
Male
Female
Tumor volume (mm³)
Time after injection (days)
B
Vehicle
Testosterone
DHT
H. Mel.
WM46
N. of cells (x10³)
Time (days)
C
Relative Proliferation
[Testosterone] (nM)
V T
P-Rb
Rb
P-ERK
ERK
β-Actin
D
MCF7
H. Mel.
WM46
YUMM1.7
Mel.290
AR
ZIP9
β-Actin
E
Free intracellular Zn++ (R.F.I. FluoZin3)
T100nM
Time (Secs)
2:00
3:40
4:04
F
Free intracellular Zn++ (R.F.I.)
Veh.
T
G
Relative Cell Proliferation
n.s.
Veh.
T
T +TPEN
H
Veh
T
T+TPEN
T+BCS
Relative Cell Proliferation
n.s.
I
Vehicle
200nM
400nM
Relative Cell Proliferation
n.s.
Zinc Pyrithione
ZnCl2
FeSO4
MnCl2

Figure 2

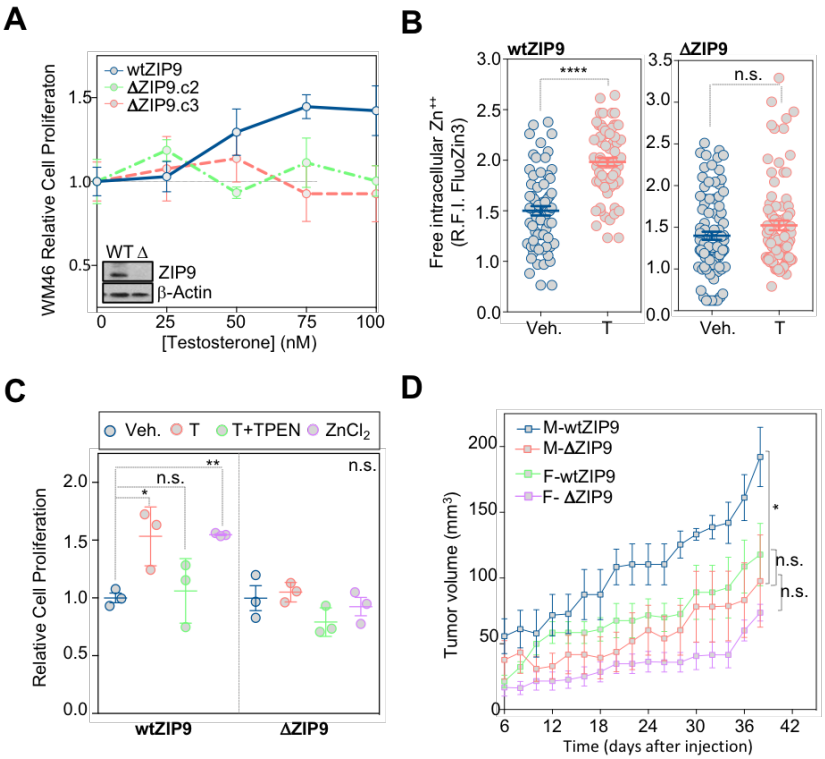
A
wtZIP9
ΔZIP9.c2
ΔZIP9.c3
WM46 Relative Cell Proliferaton
WT Δ
ZIP9
β-Actin
[Testosterone] (nM)
B
wtZIP9
ΔZIP9
Free intracellular Zn++
(R.F.I. FluoZin3)
****
n.s.
Veh.
T
C
Veh.
T
T+TPEN
ZnCl2
Relative Cell Proliferation
n.s.
*
**
n.s.
wtZIP9
ΔZIP9
D
M-wtZIP9
M-ΔZIP9
F-wtZIP9
F- ΔZIP9
Tumor volume (mm3)
*
n.s.
n.s.
Time (days after injection)

Figure 3

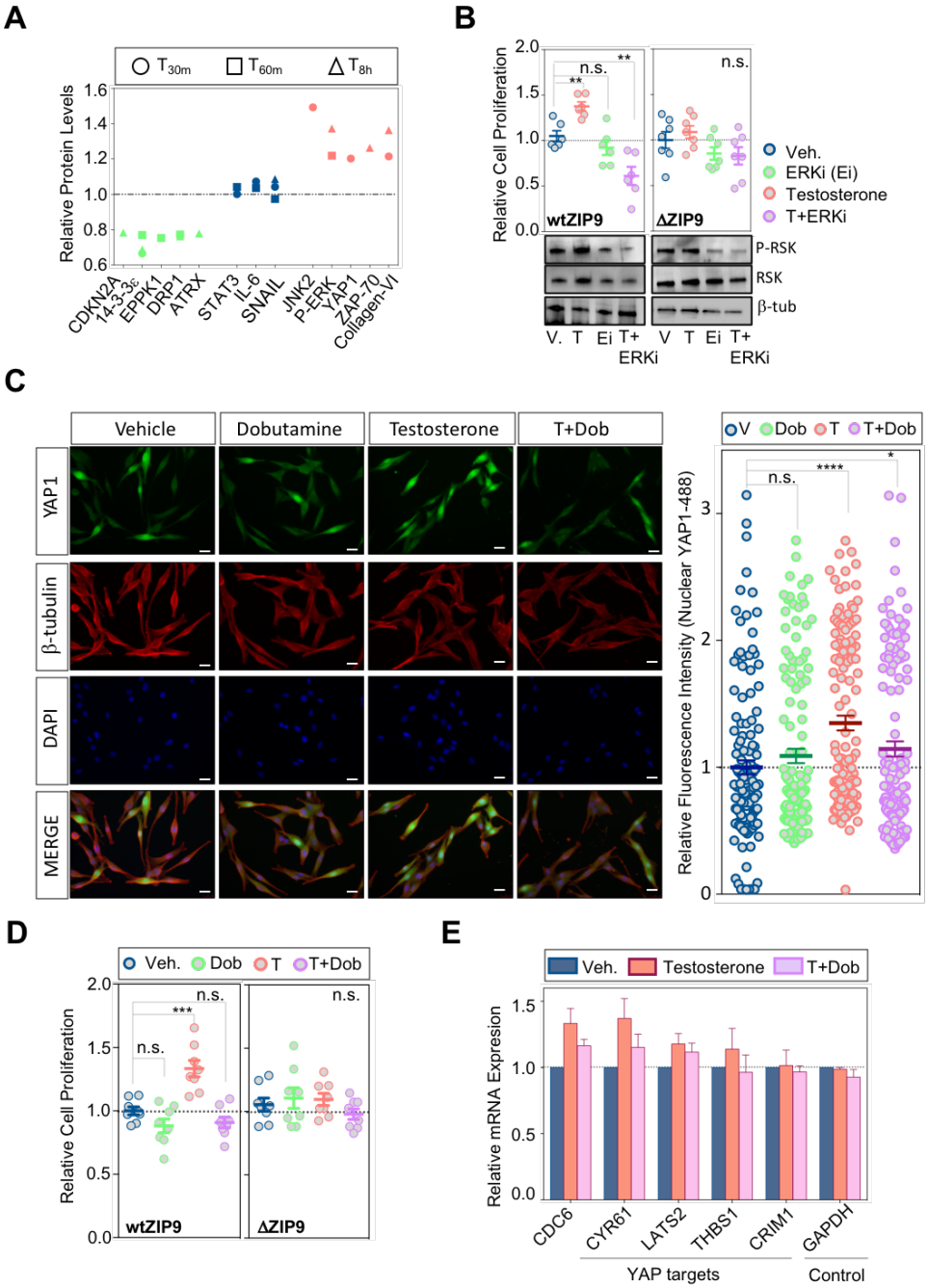
A
T30m
T60m
T8h
Relative Protein Levels
CDKN2A
14-3-3ζ
EPPK1
DRP1
ATRX
STAT3
IL-6
SNAIL
JNK2
P-ERK
YAP1
ZAP-70
Collagen-VI
B
Relative Cell Proliferation
n.s.
**
wtZIP9
ΔZIP9
Veh.
ERKi (Ei)
Testosterone
T+ERKi
P-RSK
RSK
β-tub
V. T Ei T+ ERKi
C
Vehicle
Dobutamine
Testosterone
T+Dob
YAP1
β-tubulin
DAPI
MERGE
V Dob T T+Dob
Relative Fluorescence Intensity (Nuclear YAP1-488)
****
*
D
Relative Cell Proliferation
***
E
Relative mRNA Expresion
CDC6
CYR61
LATS2
THBS1
CRIM1
GAPDH
YAP targets
Control

Figure 4

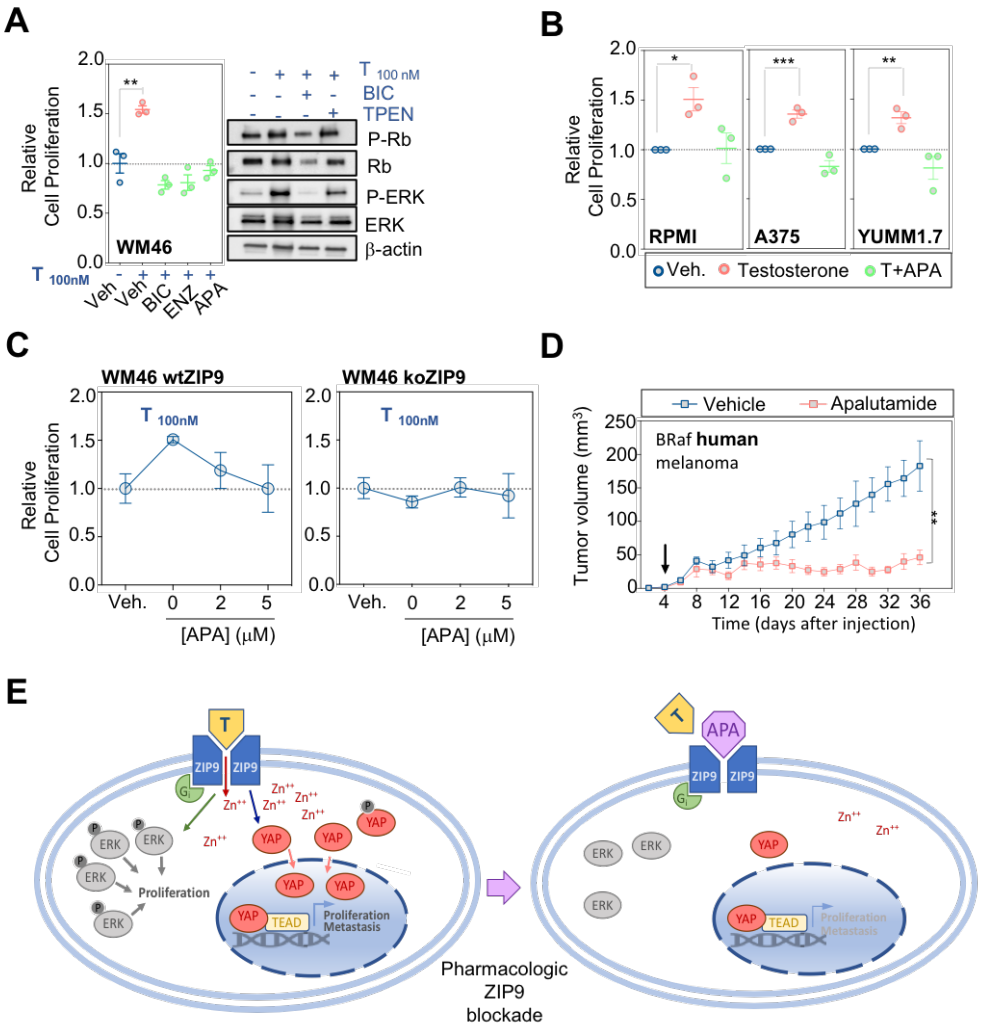

A
Relative Cell Proliferation
WM46
T 100nM
Veh
Veh+
BIC
ENZ
APA
T 100 nM
BIC
TPEN
P-Rb
Rb
P-ERK
ERK
β-actin
B
RPMI
A375
YUMM1.7
Veh.
Testosterone
T+APA
C
WM46 wtZIP9
WM46 koZIP9
[APA] (μM)
D
Vehicle
Apalutamide
BRaf human melanoma
Tumor volume (mm³)
Time (days after injection)
E
ZIP9
Proliferation
Proliferation Metastasis
TEAD
YAP
ERK
APA
Pharmacologic ZIP9 blockade

References

1. GLOBOCAN2018, (available at https://bit.ly/2Vd3C6a).

2. R. L. Siegel, K. D. Miller, A. Jemal, Cancer statistics, 2020. *CA Cancer J Clin*. 70, 7–30 (2020).

3. Surveillance, Epidemiology, and End Results Program. *SEER*, (available at https://seer.cancer.gov/index.html).

4. J. Clemmesen, T. Busk, Cancer Mortality Among Males and Females in Denmark, England, and Switzerland: V. Incidence of Accessible and Inaccessible Cancers in Danish Towns and Rural Areas. *Cancer Res*. 9, 415–421 (1949).

5. T. J. Hieken, A. E. Glasgow, E. A. L. Enninga, L. A. Kottschade, R. S. Dronca, S. N. Markovic, M. S. Block, E. B. Habermann, Sex-Based Differences in Melanoma Survival in a Contemporary Patient Cohort. *Journal of Women's Health* (2020), doi:10.1089/jwh.2019.7851.

6. GLOBOCAN. Melanoma Survival Over Time in Males vs Females., (available at shorturl.at/lyzTY).

7. C. A. Natale, J. Li, J. Zhang, A. Dahal, T. Dentchev, B. Z. Stanger, T. W. Ridky, Activation of G protein-coupled estrogen receptor signaling inhibits melanoma and improves response to immune checkpoint blockade. *Elife*. 7 (2018), doi:10.7554/eLife.31770.

8. C. A. Natale, E. K. Duperret, J. Zhang, R. Sadeghi, A. Dahal, K. T. O'Brien, R. Cookson, J. D. Winkler, T. W. Ridky, Sex steroids regulate skin pigmentation through nonclassical membrane-bound receptors. *Elife*. 5 (2016), doi:10.7554/eLife.15104.

9. M. A. Sperling, *Pediatric Endocrinology-Mean Sex Steriod Concentration in Infants, Children and adults.* (Elsevier Health Sciences, 2014; https://bit.ly/2uVOlvS).

10. A. Barbosa-Desongles, C. Hernández, R. Simó, D. M. Selva, Testosterone induces cell proliferation and cell cycle gene overexpression in human visceral preadipocytes. *Am. J. Physiol., Cell Physiol.* 305, C355-359 (2013).

11. R. Fu, J. Liu, J. Fan, R. Li, D. Li, J. Yin, S. Cui, Novel evidence that testosterone promotes cell proliferation and differentiation via G protein-coupled receptors in the rat L6 skeletal muscle myoblast cell line. *J. Cell. Physiol.* 227, 98–107 (2012).

12. D. C. Rodríguez-Lozano, A. G. Piña-Medina, V. Hansberg-Pastor, C. Bello-Alvarez, I. Camacho-Arroyo, Testosterone Promotes Glioblastoma Cell Proliferation, Migration, and Invasion Through Androgen Receptor Activation. *Front. Endocrinol.* 10 (2019), doi:10.3389/fendo.2019.00016.

13. M. Maasberg, M. Rotsch, G. Jaques, U. Enderle-Schmidt, R. Weehle, K. Havemann, Androgen receptors, androgen-dependent proliferation, and 5 alpha-reductase activity of small-cell lung cancer cell lines. *Int. J. Cancer*. 43, 685–691 (1989).

14. P. A. A. Allil, M. A. Visconti, A. M. L. C. and M. C. Isoldi, Photoperiod and Testosterone Modulate Growth and Melanogenesis of S91 Murine Melanoma. *Medicinal Chemistry* (2008), (available at http://www.eurekaselect.com/82341/article).

15. A. H. Berg, C. D. Rice, M. S. Rahman, J. Dong, P. Thomas, Identification and characterization of membrane androgen receptors in the ZIP9 zinc transporter subfamily: I. Discovery in female atlantic croaker and evidence ZIP9 mediates testosterone-induced apoptosis of ovarian follicle cells. *Endocrinology*. 155, 4237–4249 (2014).

16. W. Matsuura, T. Yamazaki, Y. Yamaguchi-Iwai, S. Masuda, M. Nagao, G. K. Andrews, T. Kambe, SLC39A9 (ZIP9) regulates zinc homeostasis in the secretory pathway: characterization of the ZIP subfamily I protein in vertebrate cells. *Biosci. Biotechnol. Biochem.* 73, 1142–1148 (2009).

17. M. Fatfat, R. A. Merhi, O. Rahal, D. A. Stoyanovsky, A. Zaki, H. Haidar, V. E. Kagan, H. Gali-Muhtasib, K. Machaca, Copper chelation selectively kills colon cancer cells through redox cycling and generation of reactive oxygen species. *BMC Cancer*. 14, 527 (2014).

18. L. He, K. Girijashanker, T. P. Dalton, J. Reed, H. Li, M. Soleimani, D. W. Nebert, ZIP8, member of the solute-carrier-39 (SLC39) metal-transporter family: characterization of transporter properties. *Mol. Pharmacol.* 70, 171–180 (2006).

19. M. F. Leal, D. Q. Calcagno, S. Demachki, P. P. Assumpção, R. Chammas, R. R. Burbano, M. de A. C. Smith, Clinical implication of 14-3-3 epsilon expression in gastric cancer. *World J. Gastroenterol.* 18, 1531–1537 (2012).

20. M. Ruas, G. Peters, The p16INK4a/CDKN2A tumor suppressor and its relatives. *Biochim. Biophys. Acta*. 1378, F115-177 (1998).

21. U. A. Germann, B. F. Furey, W. Markland, R. R. Hoover, A. M. Aronov, J. J. Roix, M. Hale, D. M. Boucher, D. A. Sorrell, G. Martinez-Botella, M. Fitzgibbon, P. Shapiro, M. J.

Wick, R. Samadani, K. Meshaw, A. Groover, G. DeCrescenzo, M. Namchuk, C. M. Emery, S. Saha, D. J. Welsch, Targeting the MAPK Signaling Pathway in Cancer: Promising Preclinical Activity with the Novel Selective ERK1/2 Inhibitor BVD-523 (Ulixertinib). *Mol. Cancer Ther.* 16, 2351–2363 (2017).

22. Y. Han, Analysis of the role of the Hippo pathway in cancer. *Journal of Translational Medicine*. 17, 116 (2019).

23. B. Zhao, L. Li, K. Tumaneng, C.-Y. Wang, K.-L. Guan, A coordinated phosphorylation by Lats and CK1 regulates YAP stability through SCFβ-TRCP. *Genes Dev*. 24, 72–85 (2010).

24. M. Fujii, Exploration of a new drug that targets YAP. *J. Biochem.* 152, 209–211 (2012).

25. A. Bulldan, V. N. Malviya, N. Upmanyu, L. Konrad, G. Scheiner-Bobis, Testosterone/bicalutamide antagonism at the predicted extracellular androgen binding site of ZIP9. *Biochim Biophys Acta Mol Cell Res*. 1864, 2402–2414 (2017).

26. S. Ponnusamy, Y. He, D.-J. Hwang, T. Thiyagarajan, R. Houtman, V. Bocharova, B. G. Sumpter, E. Fernandez, D. L. Johnson, Z. Du, L. M. Pfeffer, R. H. Getzenberg, I. J. McEwan, D. D. Miller, R. Narayanan, Orally-Bioavailable Androgen Receptor Degrader, A Potential Next-Generation Therapeutic for Enzalutamide-Resistant Prostate Cancer. *Clin. Cancer Res.* (2019), doi:10.1158/1078-0432.CCR-19-1458.

27. K. N. Chi, N. Agarwal, A. Bjartell, B. H. Chung, A. J. Pereira de Santana Gomes, R. Given, Á. Juárez Soto, A. S. Merseburger, M. Özgüroğlu, H. Uemura, D. Ye, K. Deprince, V. Naini, J. Li, S. Cheng, M. K. Yu, K. Zhang, J. S. Larsen, S. McCarthy, S. Chowdhury,

TITAN Investigators, Apalutamide for Metastatic, Castration-Sensitive Prostate Cancer. *N. Engl. J. Med.* 381, 13–24 (2019).

28. E. B. Askew, R. T. Gampe, T. B. Stanley, J. L. Faggart, E. M. Wilson, Modulation of Androgen Receptor Activation Function 2 by Testosterone and Dihydrotestosterone. *J. Biol. Chem.* 282, 25801–25816 (2007).

29. S. L. Klein, K. L. Flanagan, Sex differences in immune responses. *Nat. Rev. Immunol.* 16, 626–638 (2016).

30. Y. Ito, M. D. Sadar, Enzalutamide and blocking androgen receptor in advanced prostate cancer: lessons learnt from the history of drug development of antiandrogens. *Res Rep Urol*. 10, 23–32 (2018).